GaINeR: Geometry-Aware Implicit Neural Representation for Image Editing

Weronika Jakubowska*^{1,†} Mikołaj Zieliński*² Rafał Tobiasz*^{3,4} Krzysztof Byrski⁴ Maciej Zięba¹ Dominik Belter² Przemysław Spurek^{3,4}

¹Wrocław University of Science and Technology ²Poznań University of Technology ³IDEAS Research Institute ⁴Jagiellonian University

†weronika.jakubowska@pwr.edu.pl

*Equal contribution

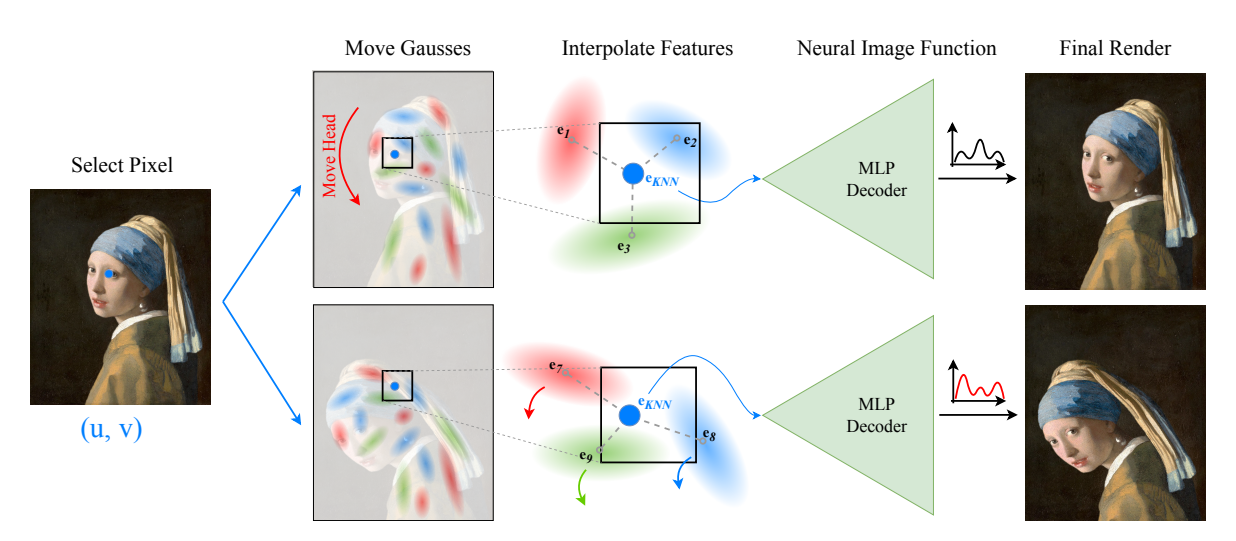


Figure 1. GaINeR enables intuitive, geometry-aware image editing by manipulating Gaussian embeddings. By moving the Gaussians in space, our encoding-decoding pipeline produces semantically consistent and photometrically coherent transformations, demonstrating controllable image editing through learned Gaussian representations.

Abstract

Implicit Neural Representations (INRs) have become an essential tool for modeling continuous 2D images, enabling high-fidelity reconstruction, super-resolution, and compression. Popular architectures such as SIREN, WIRE, and FINER demonstrate the potential of INR for capturing finegrained image details. However, traditional INRs often lack explicit geometric structure and have limited capabilities for local editing or integration with physical simulation, restricting their applicability in dynamic or interactive settings. To address these limitations, we propose GaINeR (Geometry-Aware Implicit Network Representation), a novel framework for 2D images that combines trainable Gaussian distributions with a neural network-based INR. For a given image coordinate, the model retrieves the K nearest Gaussians, aggregates distance-weighted embed-

dings, and predicts the RGB value via a neural network. This design enables continuous image representation, interpretable geometric structure, and flexible local editing, providing a foundation for physically aware and interactive image manipulation. The official implementation of our method is publicly available at https://github.com/WJakubowska/GaINeR.

1. Introduction

Implicit Neural Representations, also known as coordinate-MLPs, have fundamentally reshaped how continuous signals are represented and processed across domains ranging from computer vision to computational physics [13, 27, 29]. Unlike traditional discrete representations tied to fixed spatial resolutions, INRs parameterize signals as continu-

ous functions via neural networks, providing resolutionindependent representations with high expressiveness and memory efficiency. While several architectures, such as SIREN [27], GAUSS [23], WIRE [24], FINER [17], and positional encoding [30] have improved the ability of INRs to capture high-frequency details in images, they typically lack explicit geometric structure, limiting the possibility of local editing and integration with physical simulations.

Recent work, MiRaGe [32], addresses image editability by representing 2D images by a Gaussian Splatting-based model, enabling intuitive modifications and coupling with physics engines. Each Gaussian acts as a discrete component, allowing local transformations and perspective changes. However, because the representation is discrete, MiRaGe suffers from producing artifacts when the physical engine significantly alters the geometry of objects in a 2D image. The problem can be partially solved by training very small Gaussians, but it requires dedicated parameters that must be manually tuned. A Gaussian Splatting-based model cannot provide a truly continuous image representation.

To overcome these limitations, we propose Geometry-Aware Implicit Network Representation (GaINeR), the first model that combines the continuous representation of INR for 2D images with trainable Gaussian embeddings (see Fig. 1). GaINeR enables editing 2D images and integration with physical simulation models, see Fig. 2. We achieve this by explicitly conditioning the implicit function on a geometric structure defined by a set of specific trainable Gaussian components, each parameterized by position, scale, and a unique learnable feature embedding. The core INR network then acts as a sophisticated decoder. Given a query coordinate (x, y), the network retrieves and aggregates the features of the k nearest Gaussians using a distance-weighted mechanism, see Fig. 3. The MLP then uses this aggregated geometric and feature information to synthesize the final, high-fidelity RGB colors. This design allows precise spatial manipulation of the image, as Gaussian positions and shapes can be adjusted to produce smooth, real-time deformations. Additionally, the Gaussians can act as discrete physical entities, enabling the entire 2D representation to interact naturally with standard physics engines for dynamic simulation and animation. As a result, GaINeR achieves state-of-the-art performance in 2D image reconstruction, while maintaining fully continuous and editable representations, see Fig. 4 and experimental section.

The following constitutes a list of our key contributions:

- We introduce GaINeR, an implicit neural representation of 2D images based on Gaussian embeddings and MLPs, which provides superior reconstruction quality compared to prior INR-based approaches.
- We propose using Gaussians as feature providers conditioning an INR decoder, enabling high-fidelity and con-

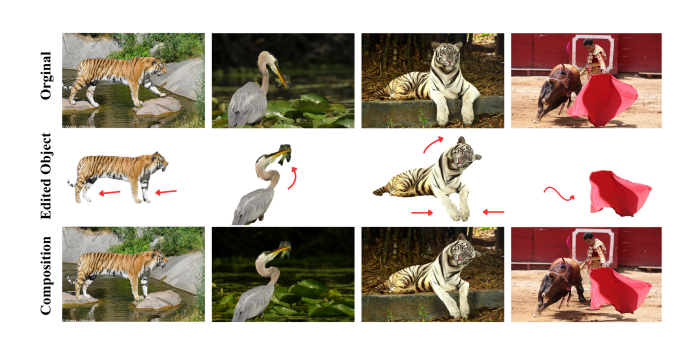


Figure 2. GaINeR produces realistic image edits by preserving structural consistency under spatial transformations. Red arrows indicate the direction of the applied changes.

tinuous color reconstruction.

 We extend the INR framework by introducing a geometric component that allows direct and flexible 2D image modification and integrates with a physical simulation engine for interactive effects.

2. Related work

Implicit Neural Representations (INRs) have received considerable attention in research [31] as neural models designed for signal representation. This paradigm has found broad application across various domains, including the representation of images [13], videos [6], and 3D shapes [22]. Significant uses span 3D shape reconstruction [19], robotics [16], and data compression [29].

INR for images INR architectures often remain simple, typically consisting of a single Multi-Layer Perceptron (MLP), with recent efforts focused on enhancing capacity through specialized embedding techniques [5, 20], unique activation functions [26], refined rendering methods [3], and regularization strategies [33].

Implicit Neural Representations (INRs), or coordinatebased MLPs, have fundamentally transformed the representation and processing of continuous signals across various domains. The main direction of INRS's development for 2D images is to adapt various activation functions and training procedures. SIREN [27] uses sine activations alongside a frequency hyperparameter ω , enabling smooth fitting and stable training. While effective for continuous signals, its fixed-frequency multiplier limits versatility, resulting in lower accuracy when modeling details across diverse frequencies [10]. GAUSS [23] employs a Gaussian activation function providing smooth localized representations that are beneficial for signal reconstruction and denoising. However, its aperiodic nature hinders the effective modeling of sharp, high-frequency details. WIRE [24] utilizes the Gabor wavelet activation, combining sinusoidal and Gaussian components to capture localized frequencies. Although effective for modeling high-frequency details within specific spatial regions, its complex-valued formulation increases computational demands, slowing both training and inference. FINER [17] modifies SIREN with a frequency-variable activation, broadening the representable frequency spectrum while retaining SIREN's benefits. However, FINER is sensitive to bias initialization and complicates the training process. Lastly, Positional Encoding (PE) [30] maps inputs into a higher-dimensional space using sinusoidal functions to mitigate the spectral bias common in MLPs.

Such a representation provides high-quality reconstruction but offers limited manual editing and integration with physical engines. In this paper, we aim to incorporate a geometric component into the INR framework to facilitate 2D image modification.

Explicit and Editable Representations Although INRs excel at compression and continuous representation, their inherent implicit nature severely limits direct interaction and editing. Conversely, explicit representations prioritize geometry and manipulability. 3D Gaussian Splatting (3DGS) [11] recently revolutionized novel view synthesis by employing a vast collection of explicit, 3D anisotropic Gaussians, achieving real-time rendering speeds. This approach naturally allows direct manipulation of Gaussian primitives, offering superior editability compared to traditional volumetric methods. Following this, Gaussian-Image [34] adapted the core GS concept to a 2D image representation, demonstrating competitive compression and quality. However, while these Gaussian-based methods introduce necessary explicit geometry, they still rely on simple color and opacity stored directly within each primitive. Consequently, they lose the continuous spatial coherence and superior color fidelity offered by a dedicated INR decoder. Models such as MiRaGe [32] attempted to address the editability challenge for 2D images by placing 2DGaussian representations in a 3D space to enable physical interactions such as bending and folding.

Our GaINeR framework distinguishes itself from these methods by creating a deeper synergy, where the explicit geometric primitives (Gaussians) are not renderers themselves, but rather rich feature providers that condition a dedicated Implicit Neural Representation decoder, thus ensuring both high-fidelity continuous color and native geometric editability and physical readiness. Examples of realistic edits enabled by our method are illustrated in Fig. 2.

3. Method

In this section, we present the GaINeR framework (see Fig. 3). We begin by revisiting the classical formulation of Implicit Neural Representations (INRs) to establish the foundational concepts. Next, we introduce GaINeR, which incorporates learnable Gaussian embeddings to achieve spa-

tially consistent and editable 2D representations. Finally, we describe the training objective and optimization strategy used to jointly learn the embedding distribution and neural decoder.

While GaINeR is introduced in the context of 2D image reconstruction and editing, its formulation is inherently dimension-agnostic. Since Gaussian embeddings and KNN-based aggregation operate in continuous Euclidean space, the same mechanism naturally extends to three-dimensional domains [20]. Consequently, GaINeR generalizes seamlessly from 2D image representations to 3D volumetric modeling, as discussed in Section 3.5.

3.1. Classical Implicit Neural Representations

Implicit Neural Representations provide a continuous and compact way to encode signals such as images, shapes, or radiance fields using neural networks. Instead of storing discrete samples (e.g., pixels or voxels), an INR models the underlying signal as a function f_{θ} that directly maps input coordinates to output values. This formulation enables subpixel-level precision, smooth interpolation, and differentiability with respect to spatial coordinates.

Formally, an INR is typically realized as a multilayer perceptron (MLP):

$$f_{\theta}: \mathbb{R}^d \to \mathbb{R}^m$$
,

where d denotes the dimensionality of the input domain (e.g., spatial coordinates), and m corresponds to the output space (e.g., color channels or density). For 2D images, the INR learns a mapping

$$f_{\theta}(x,y) = (r,q,b),$$

which associates each coordinate (x, y) with an RGB color value. In Neural Radiance Fields (NeRFs), the input extends to a 3D position and a viewing direction:

$$f_{\theta}(\mathbf{x}, \mathbf{d}) = (c, \sigma),$$

where c represents the emitted color and σ is the corresponding volume density.

This purely functional formulation captures all spatial information implicitly within the network parameters θ , without requiring discrete grids or explicit coordinate encoding. Classical INRs exhibit several key limitations. First, they lack explicit geometric structure, making it difficult to reason about spatial relationships or integrate with physical simulation engines. Second, the global nature of MLP parameterization restricts local controllability, complicating fine-grained image editing or deformation. Finally, reconstruction quality often depends on careful architectural tuning and positional encodings, which limit generalization across diverse image domains. These challenges motivate the development of geometry-aware extensions, such as our

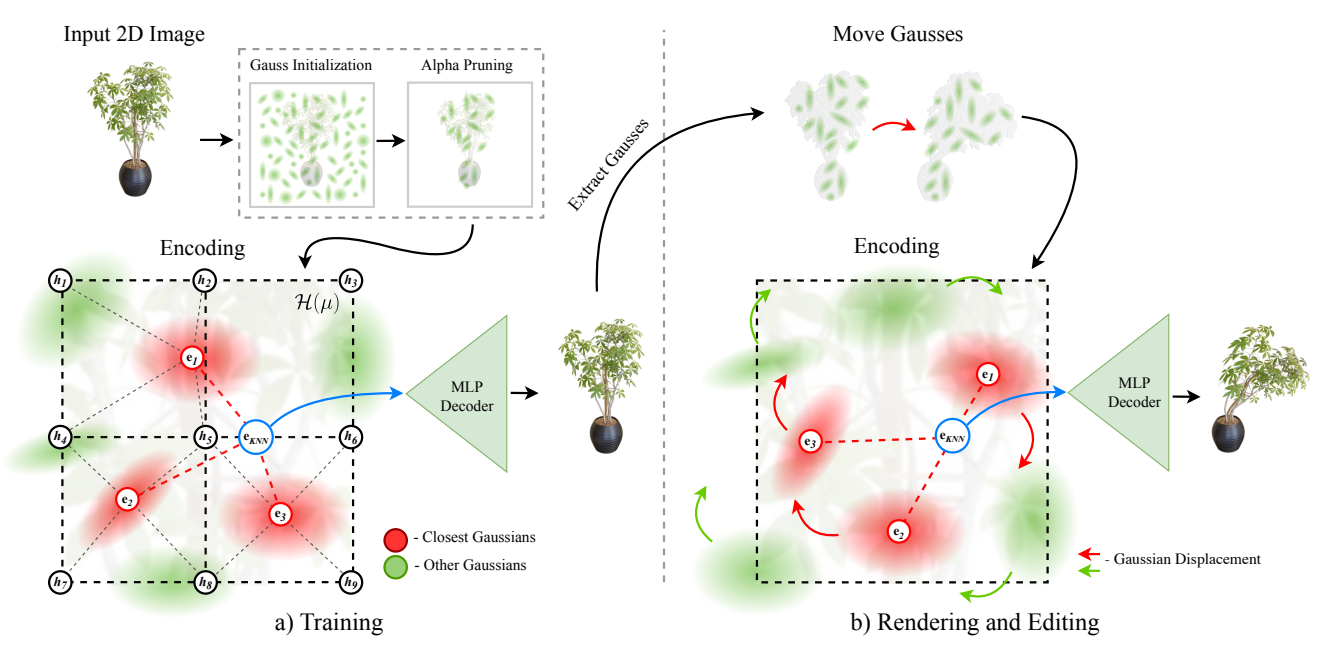


Figure 3. Overview of the GaINeR framework. (a) **Training:** For RGBA inputs, Gaussian components outside the alpha mask are removed from training. Each input coordinate \mathbf{x} is encoded via Gaussian features \mathbf{e}_i derived from the multi-resolution hashgrid $\mathcal{H}(\mu_i)$. The aggregated embedding $\mathbf{e}_{\mathrm{KNN}}(\mathbf{x},\mathcal{G})$ is obtained through radius-limited KNN interpolation and decoded by the MLP f_{θ} to reconstruct pixel color \mathbf{c} . (b) **Rendering and Editing:** After training, the optimized Gaussian set \mathcal{G} is used to reconstruct the sampling mask (for RGBA cases) and to enable spatial transformations. Edited Gaussian means $\mu_i' \in \mathbb{R}^2$ are re-encoded to produce updated embeddings $\mathbf{e}'_{\mathrm{KNN}}(\mathbf{x},\mathcal{G}')$, which the decoder maps to modified image values, enabling geometry-consistent editing.

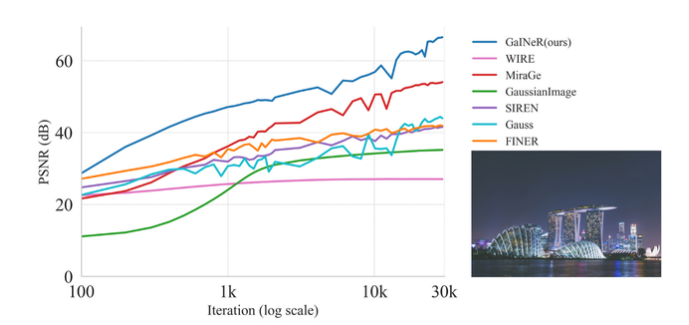


Figure 4. Comparison of PSNR obtained on a Singapore image from DIV2K dataset. All models were trained for 30 k iterations, yet our method rapidly achieves the highest PSNR within the first 1–2 k iterations, often already surpassing all other approaches.

proposed GaINeR model, which bridges implicit representations with explicit geometric priors and physical consistency.

3.2. GaINeR: Geometry-Aware Implicit Network Representation

Our proposed GaINeR extends the classical INR formulation by introducing a geometry-consistent embedding mechanism based on a family of learnable Gaussian distributions. Each 2D coordinate in the image domain is repre-

sented not as a fixed input vector, but as a continuous Gaussian embedding that encodes its local spatial context. This design enables geometry-aware reasoning and smooth interpolation while preserving the functional nature of implicit representations.

Let the input domain be $\mathbf{x}=(x,y)\in\mathbb{R}^2$. We define a set of N Gaussian components, each parameterized by its mean $\mu_i\in\mathbb{R}^2$, covariance matrix $\Sigma_i\in\mathbb{R}^{2\times 2}$, and a learnable embedding vector $\mathbf{e}_i\in\mathbb{R}^d$:

$$\mathcal{G} = \{ (\mathcal{N}_i(\mu_i, \Sigma_i), \mathbf{e}_i) \}_{i=1}^N.$$

To enhance the representational capacity of the embeddings, we are using multi-resolution hashgrid features [20] as Gaussian features obtained from, $\mathcal{H}(\mu) = \mathbf{e}$, where \mathcal{H} is hashing function. These features provide fine-grained spatial detail during training but are omitted at inference, as the learned Gaussian parameters themselves encode the required multi-scale structure.

For a given input coordinate \mathbf{x} , we identify its K nearest Gaussian centers in Euclidean space using a radius-limited k-nearest neighbors (KNN) search, where candidates are considered only within a distance r for computational efficiency. The corresponding embedding vectors of these neighbors are then aggregated using Gaussian-weighted averaging:

$$\mathbf{e_{KNN}}(\mathbf{x},\mathcal{G}) = \frac{\sum_{i \in \mathbf{KNN}(\mathbf{x},\mathcal{G})} \mathcal{N}_i(\mathbf{x}; \mu_i, \Sigma_i, \mathbf{e}_i) \, \mathbf{e}_i}{\sum_{i \in \mathbf{KNN}(\mathbf{x},\mathcal{G})} \mathcal{N}_i(\mathbf{x}; \mu_i, \Sigma_i, \mathbf{e}_i)},$$

where $KNN(x, \mathcal{G})$ denotes the indices of the K nearest neighbors of x. The resulting feature

$$\mathbf{e}(\mathbf{x}) = \mathbf{e}_{\mathbf{KNN}}(\mathbf{x}, \mathcal{G}) \in \mathbb{R}^d$$

serves as a locally geometry-aware embedding that captures both spatial proximity and the density structure of the learned Gaussians.

The aggregated embedding e(x) is subsequently processed by a multilayer perceptron (MLP) decoder:

$$f_{\theta}(\mathbf{x}) = \mathrm{MLP}_{\theta}(\mathbf{e}(\mathbf{x})),$$

where $f_{\theta}: \mathbb{R}^d \to \mathbb{R}^3$ produces the RGB color value corresponding to the coordinate \mathbf{x} . This combination of continuous Gaussian embeddings and coordinate-based neural decoding allows the model to reconstruct and edit 2D images with smooth, geometry-consistent variations.

Unlike classical INRs, which operate directly on raw spatial coordinates, GaINeR embeds each position into a learned, spatially coherent feature space. This design enhances the model's ability to capture local geometric relationships, improves reconstruction fidelity, and facilitates controllable 2D image editing through interpretable, geometry-aware embeddings.

3.3. Training Objective

The training of GaINeR jointly optimizes the parameters of the Gaussian embedding $\{(\Sigma_i, \mathbf{e}_i)\}_{i=1}^N$, the multi-resolution hashgrid encoder $\mathcal{H}(\cdot)$, and the MLP decoder f_θ that reconstructs the target image.

Given a training set $\{(\mathbf{x}_j,\mathbf{c}_j)\}_{j=1}^M$, where $M\in N$ is a subset of Gausses in training dataset, $\mathbf{x}_j=(x_j,y_j)$ denotes pixel coordinates, and $\mathbf{c}_j=(r_j,g_j,b_j)$ are the corresponding RGB values, the model is trained to minimize the Smooth L1 reconstruction loss:

$$\mathcal{L}_{\text{rec}} = \frac{1}{M} \sum_{j=1}^{M} \text{SmoothL1}(f_{\theta}(\mathbf{x}_{j}) - \mathbf{c}_{j}),$$

where

SmoothL1(
$$\mathbf{r}$$
) =
$$\begin{cases} \frac{1}{2} \|\mathbf{r}\|_2^2 / \beta, & \text{if } \|\mathbf{r}\|_1 < \beta, \\ \|\mathbf{r}\|_1 - \frac{1}{2}\beta, & \text{otherwise,} \end{cases}$$

and $\mathbf{r} = f_{\theta}(\mathbf{x}_j) - \mathbf{c}_j$ denotes the residual, while β controls the transition between the ℓ_2 and ℓ_1 regions.

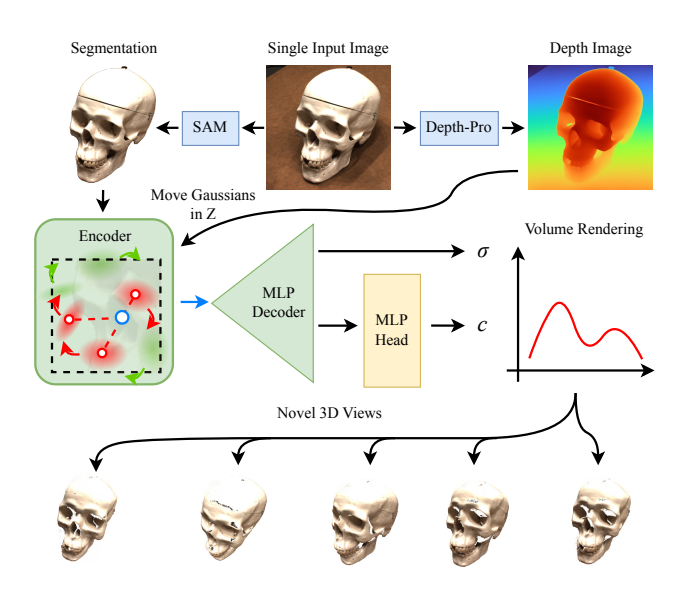


Figure 5. Overview of 3D reconstruction and rendering with GaINeR. Input images are first segmented using Segment Anything (SAM) [12] and depth is estimated with Depth-Pro [4]. The model is trained in 2D, but during inference the Gaussian means μ_i are lifted into 3D using the estimated depth values. The decoder is extended to predict both color \mathbf{c} and density σ , enabling volumetric rendering analogous to NeRF [19]. This allows the model to synthesize consistent 3D views from novel camera perspectives, as illustrated at the bottom of the figure.

Alpha-based Sampling and Mask Reconstruction. For images containing an alpha channel, i.e., RGBA inputs, we utilize the alpha map as a spatial sampling mask during training to improve computational efficiency. Specifically, only pixels with nonzero alpha values are included in the training set $\{(\mathbf{x}_j, \mathbf{c}_j)\}_{j=1}^M$, which focuses optimization on visible regions and avoids redundant computation in transparent areas.

During inference, the corresponding mask must also be reconstructed to enable consistent rendering and editing. To this end, we also train a dedicated mask model that learns to reproduce the alpha-based sampling mask. This model is subsequently animated in synchrony with the image model, ensuring temporally coherent and spatially accurate masks for all generated or edited frames.

3.4. Image Editing

During inference, the hashgrid encoder \mathcal{H} is no longer required, since the learned Gaussian embeddings \mathbf{e}_i already encode multi-scale spatial information acquired during training. Thus, the model operates directly on the optimized Gaussian parameters $\mathcal{G} = \{\mathcal{N}(\mu_i, \Sigma_i, \mathbf{e}_i)\}_{i=1}^N$, enabling efficient and interpretable scene editing.

Image editing in GaINeR is performed by modifying the spatial configuration of the Gaussian means μ_i . Because the

feature associated with any query coordinate \mathbf{x} is computed through a radius-limited KNN aggregation, $\mathbf{e_{KNN}}(\mathbf{x},\mathcal{G})$, shifting a subset of Gaussian centers $\mu_i \mapsto \mu_i'$ effectively alters the local neighborhood structure and, consequently, the interpolated feature $\mathbf{e_{KNN}}(\mathbf{x},\mathcal{G})$. The MLP decoder f_{θ} then produces a modified color field corresponding to the updated embedding distribution:

$$f'_{\theta}(\mathbf{x}) = \mathrm{MLP}_{\theta}(\mathbf{e}_{\mathbf{KNN}}(\mathbf{x}, \mathcal{G}')).$$

This formulation allows geometric transformations such as translation, rotation, bending, or stretching to be applied directly in the Gaussian space while maintaining photometric consistency in the output. Since the MLP decoder is conditioned only on the aggregated embeddings, not on absolute Gaussian positions, the model exhibits a form of spatial equivariance: moving the Gaussians induces coherent deformations in the reconstructed image without introducing artifacts.

3.5. 2D To 3D Transformations

The proposed framework (Fig. 5) naturally generalizes beyond 2D image reconstruction. By extending the MLP decoder to additionally predict a density term σ ,

$$f_{\theta}(\mathbf{x}) = (\mathbf{c}, \sigma),$$

the model integrates with a volumetric rendering formulation analogous to NeRF [19].

In this case, the rendering equation is expressed as

$$\hat{\mathbf{C}}(\mathbf{r}) = \int_{t}^{t_f} T(t) \, \sigma(\mathbf{r}(t)) \, \mathbf{c}(\mathbf{r}(t)) \, dt,$$

where,

$$T(t) = \exp\left(-\int_{t_n}^t \sigma(\mathbf{r}(s)) ds\right),$$

 $\mathbf{r}(t) = \mathbf{o} + t\mathbf{d}$ denotes a camera ray with origin \mathbf{o} and direction \mathbf{d} .

Each Gaussian component is then lifted into three-dimensional space. The local embedding for any query position \mathbf{x} is computed through the same Gaussian-weighted KNN aggregation $\mathbf{e_{KNN}}(\mathbf{x},\mathcal{G})$. As in the 2D formulation, shifting the Gaussian means $\boldsymbol{\mu}_i \mapsto \boldsymbol{\mu}_i'$ directly modifies the interpolated embedding field $\mathbf{e_{KNN}}(\mathbf{x},\mathcal{G})$, thereby altering the reconstructed volumetric scene while preserving photometric coherence.

Since the decoder f_{θ} depends solely on the aggregated embeddings rather than absolute coordinates, these transformations yield physically consistent and spatially smooth changes in appearance. Consequently, GaINeR provides a unified framework for continuous, differentiable editing across both 2D and 3D domains.

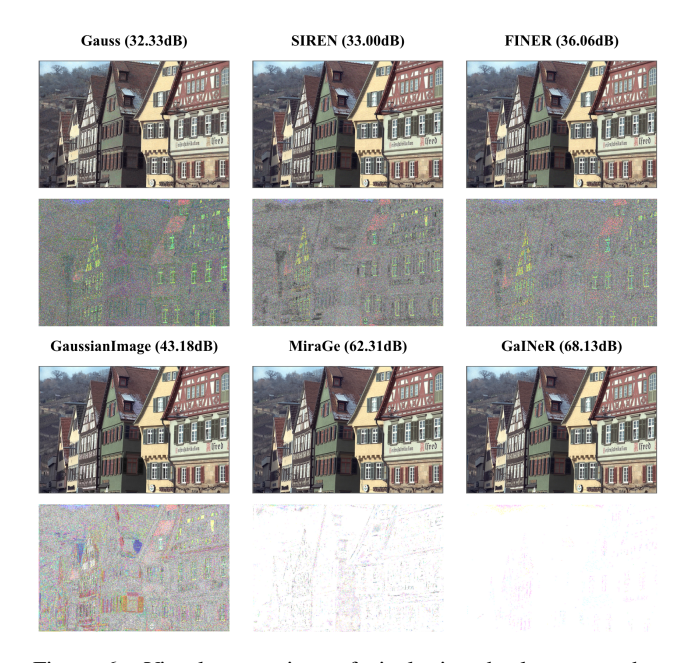


Figure 6. Visual comparison of pixel-wise absolute errors between ground truth and reconstructed images produced by our method and competing approaches. Error magnitudes are contrastenhanced using gamma correction ($\gamma = 0.2$) for better visibility.

4. Experiments

We evaluated our proposed method across three tasks: image reconstruction, image editing, and 2D-to-3D lifting. The image editing task encompassed both user-driven transformations and physically simulated deformations. For reconstruction, we employed two standard benchmarks: Kodak [9] and DIV2K [2]. The Kodak dataset contains 24 natural images of resolution 768×512 , covering diverse scenes such as portraits, landscapes, and textures. The DIV2K validation set comprises 100 high-resolution images subjected to 2x bicubic downscaling, with spatial resolutions ranging from 408 x 1020 to 1020 x 1020, and is widely used for evaluating image restoration and super-resolution methods.

4.1. Quantitative comparisons

Table 1 reports the average PSNR and MS-SSIM values obtained on both datasets. We compared our approach against WIRE [24], SIREN [27], I-NGP [20], NeuRBF [7], 3DGS [11], GaussianImage [34] and MiraGe [32]. In both cases, our method demonstrates a significant improvement in PSNR compared to previous approaches. Specifically, compared to the strongest existing method (MiraGe), our approach improves the average PSNR from 59.52 to 77.09 on the Kodak dataset, and from 54.54 to 62.20 on DIV2K, while maintaining near-perfect MS-SSIM values. This significant gain indicates that our representation captures image details with much higher fidelity and preserves struc-

Model	K	Todak	DIV2K	
1120401	PSNR↑	MS-SSIM↑	PSNR↑	MS-SSIM↑
WIRE [24]	41.47	0.9939	35.64	0.9511
SIREN [27]	40.83	0.9960	36.02	0.9568
I-NGP [20]	43.88	0.9976	37.06	0.9894
NeuRBF [7]	43.78	0.9984	37.06	0.9901
3DGS [11]	44.09	0.9991	39.12	0.9980
GaussianImage [34]	38.93	0.9984	41.48	0.9981
MiraGe [32]	59.52	0.9999	54.54	0.9998
GaINeR (ours)	77.09	0.9999	62.20	0.9999

Table 1. Quantitative comparison of our method with existing approaches on the Kodak and DIV2K datasets. Our method achieves the highest reconstruction quality across both datasets

tural consistency more effectively than prior implicit representations.

To compare performance, we trained six models (SIREN [27], WIRE [24], Gauss [23], FINER [17], GaussianImage [34] and MiraGe [32]) for 30k iterations each to ensure a fair and consistent comparison. As shown in Fig. 4, our model surpasses all competing methods already from the initial iterations, achieving significantly higher PSNR even at the earliest stages of training. Remarkably, after only about 1–2k iterations (depending on the scene), our method reaches PSNR values higher than those obtained by other approaches after 30k iterations of training.

To ensure consistency across Gaussian-based representations, we evaluate MiraGe, GaussianImage, and our proposed method under an identical training setup. Each model is initialized with 500k Gaussian primitives, which remain fixed throughout optimization (no densification or pruning), and is trained for 30k iterations. As reported in Table 2 our method achieves the highest accuracy among all evaluated approaches.

Model	Koda	ık dataset	DIV2K dataset	
1710401	PSNR↑	MS-SSIM↑	PSNR↑	MS-SSIM↑
GaussianImage [34]	30.46	0.9635	28.58	0.9565
MiraGe [32]	62.49	0.9999	58.45	0.9999
GaINeR (ours)	77.09	0.9999	62.20	0.9999

Table 2. Comparison of Gaussian-based methods evaluated using a unified configuration of 500k Gaussians (no densification) and 30k optimization iterations. Our method achieves the best performance.

4.2. Qualitative comparisons

Since the PSNR values across all methods are exceptionally high, the visual differences are barely perceptible to the human eye. Therefore, we compute the *absolute error* for each pixel and visualize the results as error maps, shown in Fig. 6. These error visualizations reveal that GaINeR method produces almost no noticeable errors compared to

other approaches, demonstrating its superior reconstruction accuracy and stability.

4.3. Editing comparisons

We conducted a series of experiments on images from the DIV2K dataset, exploring various types of spatial modifications. For consistency across methods, we evaluate MiraGe using two camera configurations: one and mirror. The one camera setup corresponds to the same viewpoint configuration employed in our GaINeR model, ensuring direct comparability. The mirror camera provides a reflective viewpoint that captures mirrored scene geometry and appearance. As illustrated in Fig. 7, we evaluate the visual effects of bending, stretching, cutting and displacing Gaussian components. MiraGe exhibits severe distortions under these transformations, primarily due to its reliance on Gaussian primitives for direct rendering. In contrast, our GaINeR framework produces visually consistent and realistic results across all conditions, as it utilizes Gaussian components solely for encoding rather than for rendering.

4.4. Physics comparisons

To demonstrate applicability in dynamic scenarios, we treat the centers of our learned Gaussians as material points in a Material Point Method (MPM) simulation driven by the Taichi Elements [28] engine. Fig. 8 compares our method against MiraGe, with full animations provided in the supplementary material. The results highlight the benefits of our continuous representation. The results show that MiraGe's discrete representation produces geometric artifacts under deformation. In contrast, GaINeR renders coherent surfaces even under significant deformation. Since our MLP decoder is conditioned on the geometric structure, it can robustly interpolate visual information from sparse or distorted particle distributions, avoiding the visual discontinuities inherent to discrete representations.

4.5. 2D-to-3D Lifting

We performed a series of experiments demonstrating the capability of GaINeR to lift 2D representations into 3D space. As illustrated in Fig. 9, GaINeR reconstructs realistic and geometrically consistent 3D models by leveraging the spatially coherent nature of Gaussian embeddings and the KNN-based aggregation mechanism extended to three dimensions.

We evaluated our method on various objects from the Tanks and Temples [14], LLFF [18], and DTU [1] datasets (see also Fig. 5). Due to the continuity of the Gaussian representation in 3D, GaINeR also produces accurate depth maps for rendered views. For these experiments, depth supervision was provided using depth maps estimated by Depth-Pro [4], which were normalized to ensure consistent metric ranges across datasets.

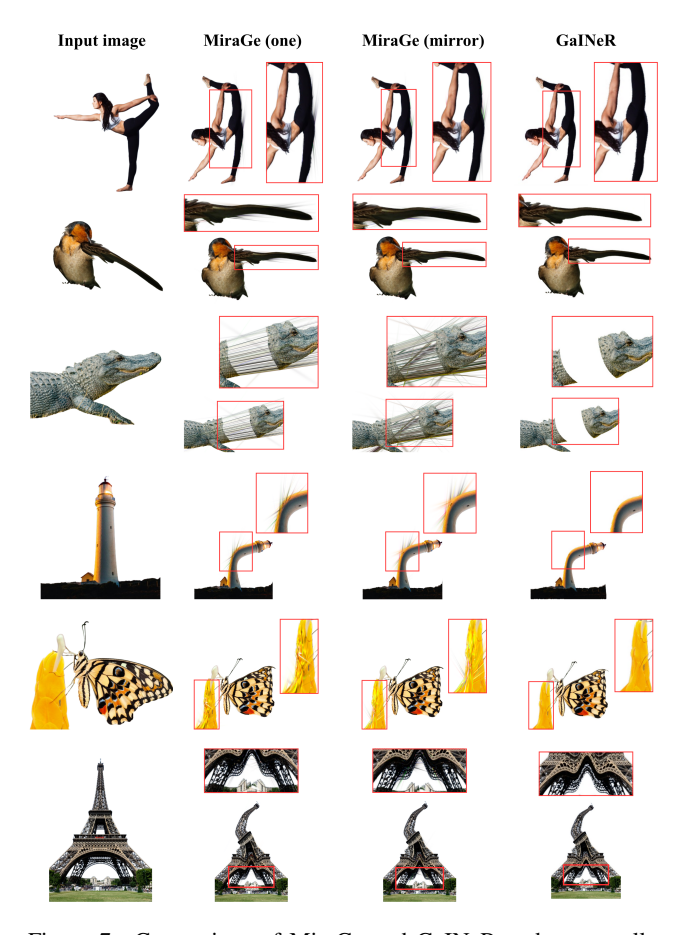


Figure 7. Comparison of MiraGe and GaINeR under manually applied geometric modifications in Blender. GaINeR maintains stable and realistic results under bending, cutting and stretching, whereas MiraGe exhibits visible artifacts.

Overall, GaINeR demonstrates strong performance in reconstructing and rendering 3D geometry from 2D inputs, achieving realistic depth perception and spatial coherence.

5. Conclusion

In this work, we introduced GaINeR, a geometry-aware implicit representation that combines the continuous flexibility of neural networks with the structured expressiveness of learnable Gaussian embeddings. By encoding spatial coordinates through Gaussian-weighted KNN aggregation, GaINeR achieves smooth, spatially coherent reconstructions while enabling 2D image manipulations.

Our framework bridges coordinate-based MLPs with explicit geometric priors, yielding a unified model capable of high-fidelity reconstruction and photometrically consistent transformations. Comprehensive experiments demonstrate that GaINeR surpasses prior implicit representations such as SIREN, WIRE, and MiraGe in both quantitative accuracy and visual quality, while offering greater interpretabil-

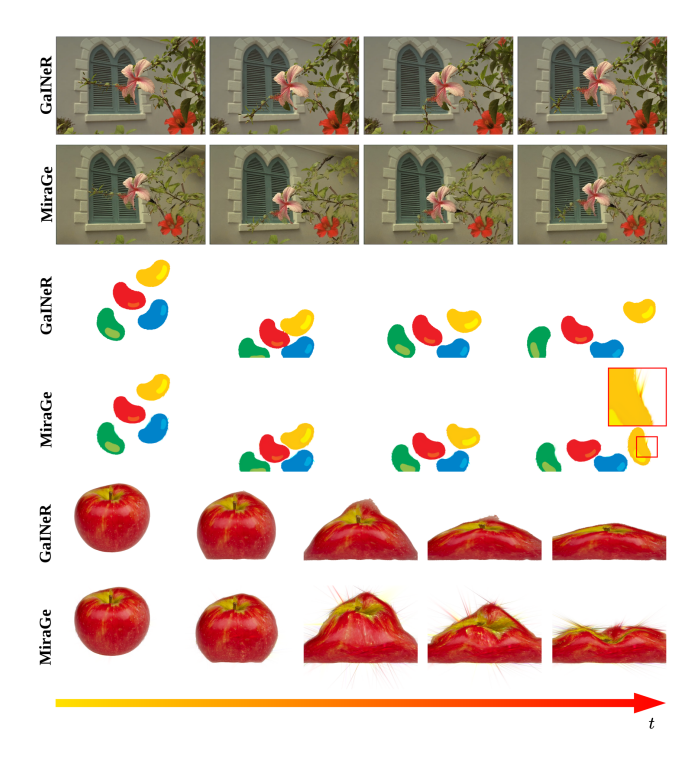


Figure 8. Qualitative comparison of physics-based animations. **Elastic Flower:** MiraGe's render exhibits transparencies, while ours remains opaque. **Elastic Beans:** MiraGe produces spiky boundary artifacts, which are absent in our result. **Sand Apple:** As the object disintegrates, MiraGe's rendering again shows structural artifacts, unlike GaINeR.

ity through its Gaussian-based encoding.

Furthermore, we extend the formulation to 2D-to-3D lifting, where the learned Gaussian embeddings are projected into three-dimensional space to reconstruct depth-aware geometry and novel viewpoints from a single image. This generalization highlights the potential of Gaussian-encoded neural fields for bridging 2D perception and 3D reasoning, paving the way for future research in continuous, geometry-aware scene representations.

6. Acknowledgment

The work of W. Jakubowska and P. Spurek was supported by the National Centre of Science (Poland) Grant No. 2023/50/E/ST6/00068. M. Zieliński and D. Belter were supported by the National Science Centre, Poland, under research project no UMO-2023/51/B/ST6/01646. The scientific work was carried out using the infrastructure of the Poznan Supercomputing and Networking Center.

References

H. Aanæs, A.L. Dahl, and K. Steenstrup Pedersen. Interesting interest points. *International Journal of Computer Vision*, 97:18–35, 2012.



Figure 9. Results of 2D-to-3D lifting with GaINeR. Objects are rendered from multiple novel viewpoints (left to right), and the corresponding depth maps are shown in the top-left corners of each rendering. Some floaters appear due to the inconsistencies in generated depth maps by Depth-Pro.

- [2] Eirikur Agustsson and Radu Timofte. Ntire 2017 challenge on single image super-resolution: Dataset and study. In *The IEEE Conference on Computer Vision and Pattern Recognition (CVPR) Workshops*, 2017. 6, 11, 13, 14
- [3] Jonathan T Barron, Ben Mildenhall, Matthew Tancik, Peter Hedman, Ricardo Martin-Brualla, and Pratul P Srinivasan. Mip-nerf: A multiscale representation for anti-aliasing neural radiance fields. In *Proceedings of the IEEE/CVF international conference on computer vision*, pages 5855–5864, 2021. 2
- [4] Alexey Bochkovskiy, Amaël Delaunoy, Hugo Germain, Marcel Santos, Yichao Zhou, Stephan R. Richter, and Vladlen Koltun. Depth pro: Sharp monocular metric depth in less than a second. In *ICLR*. OpenReview.net, 2025. 5, 7
- [5] Anpei Chen, Zexiang Xu, Andreas Geiger, Jingyi Yu, and Hao Su. Tensorf: Tensorial radiance fields. In *European conference on computer vision*, pages 333–350. Springer, 2022.
- [6] Zeyuan Chen, Yinbo Chen, Jingwen Liu, Xingqian Xu, Vidit Goel, Zhangyang Wang, Humphrey Shi, and Xiaolong Wang. Videoinr: Learning video implicit neural representation for continuous space-time super-resolution. In *Proceed*-

- ings of the IEEE/CVF Conference on Computer Vision and Pattern Recognition, pages 2047–2057, 2022. 2
- [7] Zhang Chen, Zhong Li, Liangchen Song, Lele Chen, Jingyi Yu, Junsong Yuan, and Yi Xu. Neurbf: A neural fields representation with adaptive radial basis functions, 2023. 6, 7
- [8] Blender Online Community. Blender a 3d modelling and rendering package, 2018. 11
- [9] Eastman Kodak Company. Kodak lossless true color image suite. Web page, 1991. Available at https://rok.us/ graphics/kodak/. 6
- [10] Adam Kania, Marko Mihajlovic, Sergey Prokudin, Jacek Tabor, and Przemysław Spurek. Fresh: Frequency shifting for accelerated neural representation learning. In *The Thirteenth International Conference on Learning Represen*tations, 2025. 2
- [11] Bernhard Kerbl, Georgeios Kopanas, Thomas Leimkühler, and George Drettakis. 3d gaussian splatting for real-time radiance field rendering. ACM Transactions on Graphics, 42 (4), 2023. 3, 6, 7
- [12] Alexander Kirillov, Eric Mintun, Nikhila Ravi, Hanzi Mao, Chloé Rolland, Laura Gustafson, Tete Xiao, Spencer Whitehead, Alexander C. Berg, Wan-Yen Lo, Piotr Dollár, and Ross B. Girshick. Segment anything. In *ICCV*, pages 3992– 4003. IEEE, 2023. 5
- [13] Sylwester Klocek, Łukasz Maziarka, Maciej Wołczyk, Jacek Tabor, Jakub Nowak, and Marek Śmieja. Hypernetwork functional image representation. In *International Conference* on Artificial Neural Networks, pages 496–510. Springer, 2019. 1, 2
- [14] Arno Knapitsch, Jaesik Park, Qian-Yi Zhou, and Vladlen Koltun. Tanks and temples: Benchmarking large-scale scene reconstruction. ACM Transactions on Graphics, 36(4), 2017.
- [15] Black Forest Labs, Stephen Batifol, Andreas Blattmann, Frederic Boesel, Saksham Consul, Cyril Diagne, Tim Dockhorn, Jack English, Zion English, Patrick Esser, Sumith Kulal, Kyle Lacey, Yam Levi, Cheng Li, Dominik Lorenz, Jonas Müller, Dustin Podell, Robin Rombach, Harry Saini, Axel Sauer, and Luke Smith. Flux.1 kontext: Flow matching for in-context image generation and editing in latent space, 2025. 11
- [16] Chen-Hsuan Lin, Wei-Chiu Ma, Antonio Torralba, and Simon Lucey. Barf: Bundle-adjusting neural radiance fields. In Proceedings of the IEEE/CVF international conference on computer vision, pages 5741–5751, 2021. 2
- [17] Zhen Liu, Hao Zhu, Qi Zhang, Jingde Fu, Weibing Deng, Zhan Ma, Yanwen Guo, and Xun Cao. Finer: Flexible spectral-bias tuning in implicit neural representation by variable-periodic activation functions. In *Proceedings of* the IEEE/CVF Conference on Computer Vision and Pattern Recognition, pages 2713–2722, 2024. 2, 3, 7, 14
- [18] Ben Mildenhall, Pratul P. Srinivasan, Rodrigo Ortiz-Cayon, Nima Khademi Kalantari, Ravi Ramamoorthi, Ren Ng, and Abhishek Kar. Local light field fusion: Practical view synthesis with prescriptive sampling guidelines. ACM Transactions on Graphics (TOG), 2019. 7
- [19] Ben Mildenhall, Pratul P Srinivasan, Matthew Tancik, Jonathan T Barron, Ravi Ramamoorthi, and Ren Ng. Nerf:

- Representing scenes as neural radiance fields for view synthesis. *Communications of the ACM*, 65(1):99–106, 2021. 2, 5, 6
- [20] Thomas Müller, Alex Evans, Christoph Schied, and Alexander Keller. Instant neural graphics primitives with a multiresolution hash encoding. ACM transactions on graphics (TOG), 41(4):1–15, 2022. 2, 3, 4, 6, 7
- [21] Open AI. Gpt image 1. pen AI, 2025. https: //platform.openai.com/docs/models/gptimage-1.11
- [22] Jeong Joon Park, Peter Florence, Julian Straub, Richard Newcombe, and Steven Lovegrove. Deepsdf: Learning continuous signed distance functions for shape representation. In *Proceedings of the IEEE/CVF conference on computer vision and pattern recognition*, pages 165–174, 2019. 2
- [23] Sameera Ramasinghe and Simon Lucey. Beyond periodicity: Towards a unifying framework for activations in coordinatemlps. In *European Conference on Computer Vision*, pages 142–158. Springer, 2022. 2, 7, 14
- [24] Vishwanath Saragadam, Daniel LeJeune, Jasper Tan, Guha Balakrishnan, Ashok Veeraraghavan, and Richard G Baraniuk. Wire: Wavelet implicit neural representations. In Proceedings of the IEEE/CVF Conference on Computer Vision and Pattern Recognition, pages 18507–18516, 2023. 2, 6, 7, 14
- [25] Team Seedream, :, Yunpeng Chen, Yu Gao, Lixue Gong, Meng Guo, Qiushan Guo, Zhiyao Guo, Xiaoxia Hou, Weilin Huang, Yixuan Huang, Xiaowen Jian, Huafeng Kuang, Zhichao Lai, Fanshi Li, Liang Li, Xiaochen Lian, Chao Liao, Liyang Liu, Wei Liu, Yanzuo Lu, Zhengxiong Luo, Tongtong Ou, Guang Shi, Yichun Shi, Shiqi Sun, Yu Tian, Zhi Tian, Peng Wang, Rui Wang, Xun Wang, Ye Wang, Guofeng Wu, Jie Wu, Wenxu Wu, Yonghui Wu, Xin Xia, Xuefeng Xiao, Shuang Xu, Xin Yan, Ceyuan Yang, Jianchao Yang, Zhonghua Zhai, Chenlin Zhang, Heng Zhang, Qi Zhang, Xinyu Zhang, Yuwei Zhang, Shijia Zhao, Wenliang Zhao, and Wenjia Zhu. Seedream 4.0: Toward next-generation multimodal image generation, 2025. 11
- [26] Vincent Sitzmann, Eric Chan, Richard Tucker, Noah Snavely, and Gordon Wetzstein. Metasdf: Meta-learning signed distance functions. Advances in Neural Information Processing Systems, 33:10136–10147, 2020. 2
- [27] Vincent Sitzmann, Julien Martel, Alexander Bergman, David Lindell, and Gordon Wetzstein. Implicit neural representations with periodic activation functions. *Advances in neural* information processing systems, 33:7462–7473, 2020. 1, 2, 6, 7, 14
- [28] Taichi Graphics. Taichi elements: A high-performance multi-material continuum physics engine. GitHub repository, 2020. https://github.com/taichi-dev/taichi_elements.7,12
- [29] Towaki Takikawa, Shunsuke Saito, James Tompkin, Vincent Sitzmann, Srinath Sridhar, Or Litany, and Alex Yu. Neural fields for visual computing: Siggraph 2023 course. In ACM SIGGRAPH 2023 Courses, pages 1–227. 2023. 1, 2
- [30] Matthew Tancik, Pratul Srinivasan, Ben Mildenhall, Sara Fridovich-Keil, Nithin Raghavan, Utkarsh Singhal, Ravi Ramamoorthi, Jonathan Barron, and Ren Ng. Fourier features

- let networks learn high frequency functions in low dimensional domains. *Advances in neural information processing systems*, 33:7537–7547, 2020. 2, 3
- [31] Ayush Tewari, Justus Thies, Ben Mildenhall, Pratul Srinivasan, Edgar Tretschk, Wang Yifan, Christoph Lassner, Vincent Sitzmann, Ricardo Martin-Brualla, Stephen Lombardi, et al. Advances in neural rendering. In *Computer Graphics Forum*, pages 703–735. Wiley Online Library, 2022. 2
- [32] Joanna Waczynska, Tomasz Szczepanik, Piotr Borycki, Slawomir Tadeja, Thomas Bohné, and Przemysław Spurek. Mirage: Editable 2d images using gaussian splatting. In Forty-second International Conference on Machine Learning, 2025. 2, 3, 6, 7, 11, 13, 14, 15
- [33] Jiawei Yang, Marco Pavone, and Yue Wang. Freenerf: Improving few-shot neural rendering with free frequency regularization. In *Proceedings of the IEEE/CVF conference on computer vision and pattern recognition*, pages 8254–8263, 2023.
- [34] Xinjie Zhang, Xingtong Ge, Tongda Xu, Dailan He, Yan Wang, Hongwei Qin, Guo Lu, Jing Geng, and Jun Zhang. Gaussianimage: 1000 fps image representation and compression by 2d gaussian splatting. In *European Conference on Computer Vision*, pages 327–345. Springer, 2024. 3, 6, 7, 14

Supplementary materials:

GaINeR: Geometry-Aware Implicit Neural Representation for Image Editing

Weronika Jakubowska^{*1,†} Mikołaj Zieliński^{*2} Rafał Tobiasz^{*3,4} Krzysztof Byrski⁴ Maciej Zięba¹ Dominik Belter² Przemysław Spurek^{3,4}

¹Wrocław University of Science and Technology ²Poznań University of Technology ³IDEAS Research Institute ⁴Jagiellonian University

†weronika.jakubowska@pwr.edu.pl

*Equal contribution

7. Extended Experimental Analysis

This section presents additional experiments that complement the main results. It begins by outlining the difficulties encountered by prompt-based LLM and diffusion editors when performing controlled geometric modifications. This is followed by further editing examples, physics-inspired manipulations, and an ablation study. Together, these extended results provide a broader view of the method's capabilities and behavior.

7.1. Limitations of Prompt-Based LLM and Diffusion Editors

Recent LLM- and diffusion-based editors enable high-level semantic modifications, but they lack geometric controllability and often introduce unpredictable artifacts when altering object shape, scale, or structure. Because these models operate through generative resampling, they do not preserve underlying geometry and offer limited support for continuous, user-defined transformations or temporally stable animation. As illustrated in Fig. 10, methods such as GPT-IMAGE-1 [21], Flux [15] and Seedream 4.0 [25] fail to perform even simple geometric edits, consistently producing shape distortions or hallucinated content. In contrast, our INR-based representation provides a continuous, functionlevel encoding that enables precise and deterministic geometric edits including bending, stretching, and scaling without altering object identity or introducing hallucinated content.

7.2. Error Comparisons

In this section, we provide additional examples illustrating the absolute pixel-wise error produced by our method compared to baseline approaches (see Fig. 11). The visualizations highlight areas where reconstruction discrepancies are most pronounced and allow for a detailed qualitative assessment of image fidelity. We present results on several images from the DIV2K validation set [2], which we used for evaluation. These examples demonstrate that our model consis-



Figure 10. Comparison of geometric edit performance across models. Starting from a generated image of a cat, each method was asked to apply the prompt: "Enlarge only the cat's left ear by about 150%, keeping the rest of the cat completely unchanged." For our method, the edit was applied directly through our representation using a controlled geometric transformation implemented in Blender. GaINeR method produces a clean, targeted edit while keeping the cat's appearance intact. In contrast, Flux cuts off part of the ear, Seedream enlarges the ear but also scales the whole cat, and GPT-IMAGE-1 makes the ear much larger than requested. This shows that prompt-based generative editors struggle with simple geometric edits.

tently produces minimal reconstruction errors, preserving fine details and textures even in challenging regions.

7.3. Editing Comparisons

In Fig. 15, we provide additional qualitative comparisons illustrating how the models respond to a broader range of manual geometric modifications. These examples primarily involve bending and, in some cases, moderate stretching performed in Blender [8]. Across most scenarios, the GaINeR maintains stable geometry and appearance, producing visually coherent results even under stronger or more irregular deformations. MiraGe [32] occasionally exhibits structural inconsistencies under such modifications; however, in several examples both approaches perform comparably well.

To further illustrate the flexibility of the editing process, Fig. 12 shows an example in which the extracted object is manually modified and subsequently placed into a newly generated background. This workflow enables pre-

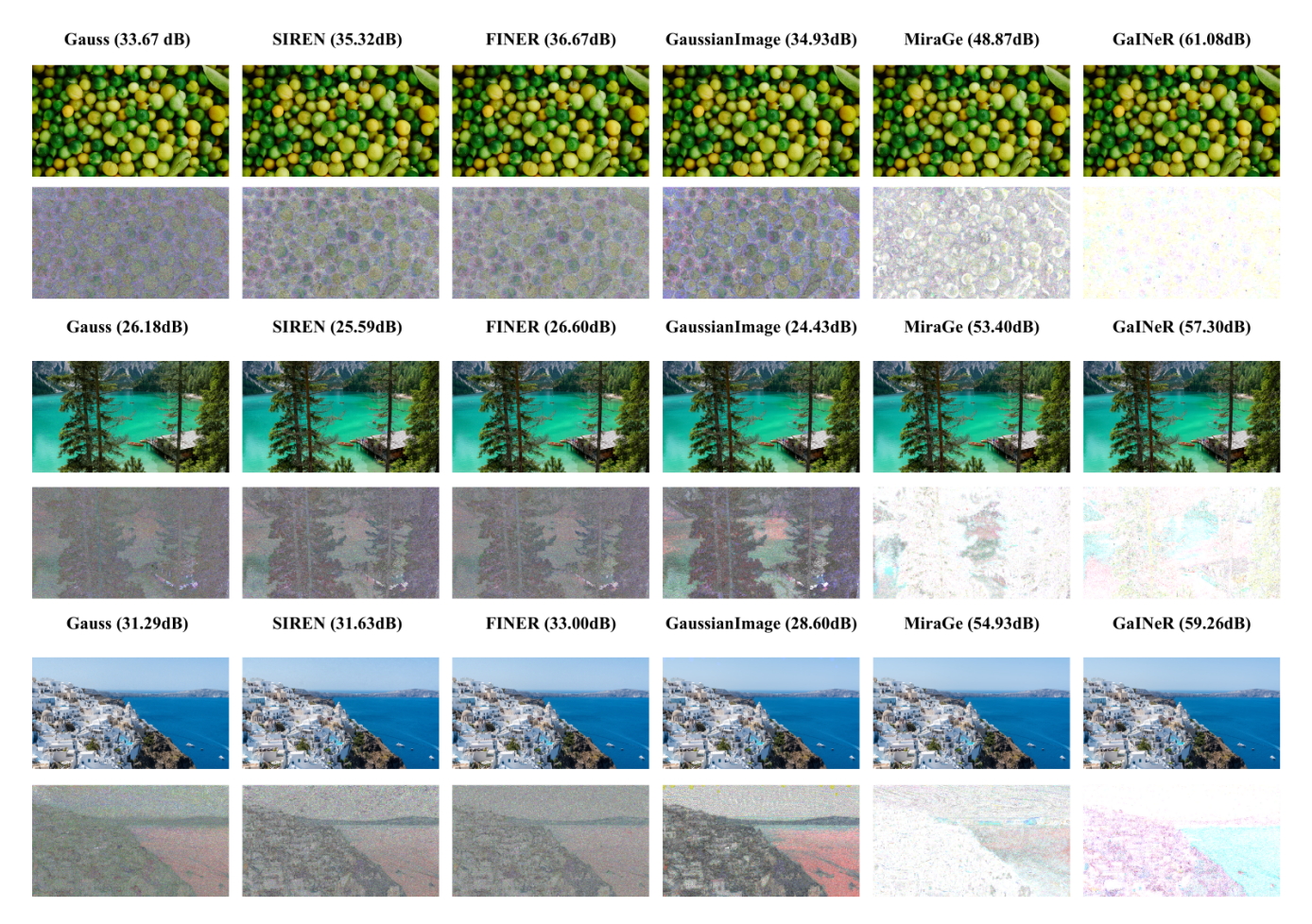


Figure 11. Visual comparison of pixel-wise absolute errors between ground truth and reconstructed images produced by our method and competing approaches. Error magnitudes are contrast-enhanced using gamma correction ($\gamma = 0.2$) for better visibility.

cise, user-controlled adjustments while preserving consistency between the modified object and the environment.

To further assess the model's behavior under simple geometric edits, we change the scale of the main object in the image by either enlarging or shrinking it. As shown in Fig. 13, these operations do not introduce visual artifacts, and the object remains structurally continuous and visually consistent in both cases.

Beyond static manual edits, the editing pipeline also supports generating animations in Blender, enabling controlled simulations of various object motions. By applying frame-wise geometric transformations, we can assess the temporal stability of the reconstruction process. As illustrated in Fig. 14, GaINeR maintains structural coherence and produces artifact-free frames throughout the animated sequence, demonstrating its robustness under continuous, motion-induced transformations.

7.4. Physics Evaluations

We further investigate the dynamic capabilities of GaINeR through three distinct simulation scenarios powered by the Taichi Elements engine [28]. These experiments demonstrate the versatility of our explicit Gaussian embeddings when utilized as physical particles.

First, we validate baseline elastic deformation under constant gravity (Fig. 16, top), ensuring that the learned representation maintains volumetric consistency during collision. Second, we introduce temporally varying external forces to a complex structure (Fig. 16, middle), demonstrating that the decoder produces artifact-free renderings even under oscillating bending deformations.

Finally, we explore complex multi-material interactions within a single scene (Fig. 16, bottom). Leveraging the explicit spatial coordinates of GaINeR, we segment a single trained image representation into distinct regions based on pixel position. Gaussians corresponding to the text were assigned granular (sand) material properties, while the up-

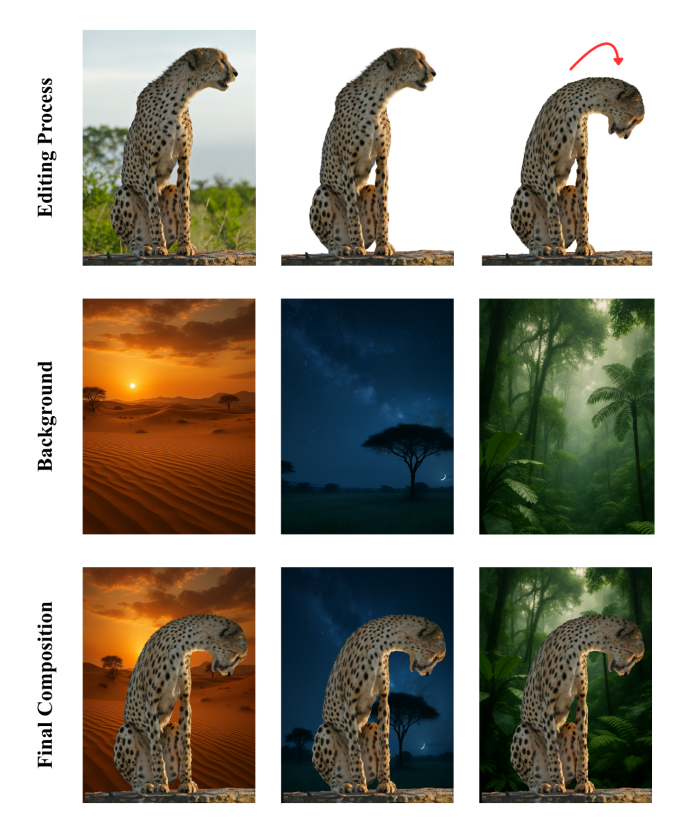


Figure 12. Object extraction, manual editing in Blender, and background replacement produced using GaINeR. The edited object is reintegrated into a newly generated scene while maintaining visual consistency.

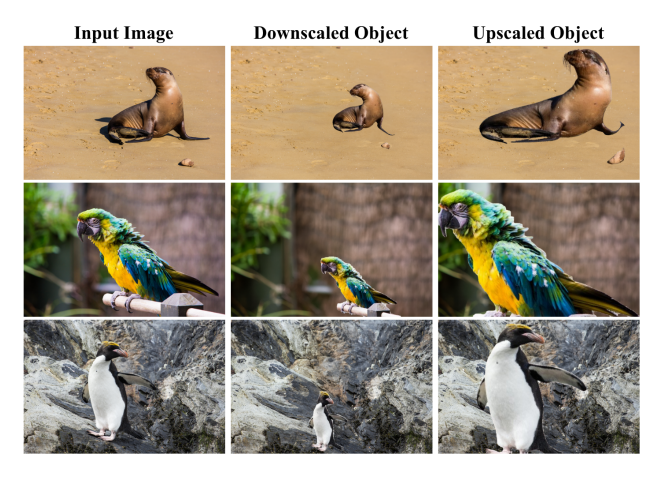


Figure 13. GaINeR tested under scale-based geometric modifications, including object enlargement and reduction. In all cases, the method yields stable and visually coherent results.

per region was assigned fluid (water) properties. This confirms that GaINeR allows for spatially-aware semantic assignment of physical parameters, enabling diverse materials to interact seamlessly within a unified simulation.

7.5. Object Integration and Compositing

We compare the workflow for integrating edited foreground objects with backgrounds in GaINeR versus MiRaGe [32].

Based on the collage capabilities presented in [32], Mi-RaGe typically handles multi-object integration by arranging Gaussian primitives within a shared 3D space. Consequently, the final image is produced via a single rasterization pass. This approach relies heavily on the splatting engine to handle depth sorting and occlusion. However, as observed in the qualitative comparisons in our main paper (see physics simulation figures), this approach can lead to unintended transparency artifacts. Since the object is represented as a cloud of discrete primitives without a continuous surface mesh, deformation (such as stretching) can create gaps between Gaussians or reduce accumulated density, causing the background to bleed through the foreground object.

In contrast, our framework adopts a layer-based compositing workflow. We learn a precise, continuous alpha mask of the object alongside its RGB appearance. The modified object is rendered together with its mask to produce explicit color and alpha channels. The final scene is assembled by alpha-blending the rendered foreground over the inpainted background.

By explicitly separating foreground reconstruction from background integration, GaINeR ensures crisp object boundaries and maintains solid opacity. Even under significant deformation, the learned alpha mask ensures the object fully occludes the background, eliminating the "ghosting" or transparency artifacts observed in the baseline methods.

7.6. Size and Time Comparisons

We compare the computational characteristics of GaINeR with several representative baselines, reporting training time, inference throughput, and model size. To ensure consistency across methods with differing input-size constraints, all models were trained on the DIV2K dataset [2] subjected to $3\times$ bicubic downscaling. Training was performed on an NVIDIA RTX 5090 GPU, except for MiraGe [32], which requires older CUDA support and was therefore trained on an NVIDIA RTX 3090. For GaINeR, we report only the components required at inference (excluding optimizers, training buffers, and hash-grid encoders) so that the model size reflects the minimal representation used for rendering.

The results in Tab. 3 expose a clear trade-off between editability, reconstruction quality, and runtime/storage costs. Only MiraGe and GalNeR provide native editability. These two methods also achieve the highest PSNR in our experiments, indicating that editability in our setting did not come at the expense of reconstruction fidelity. However, this capability incurs a computational cost: both editable models have substantially larger serialized footprints and slower



Figure 14. Sequences generated in Blender through frame-wise geometric transformations demonstrate that the method maintains stable structure and visual consistency throughout the animation.

end-to-end performance compared to lightweight baselines (SIREN [27], FINER [17], Gauss [23]) and extremely compact pipelines (GaussianImage [34]). Notably, our primary editable baseline, MiraGe, is more than twice as large as our model and, due to its densification process, does not maintain a constant representation size during training, whereas our method preserves a fixed and compact footprint throughout.

Model		Size [MB]		
	Train [s]	Inference [FPS]		
WIRE [24]	410	34.01	0.76	
SIREN [27]	89	163.90	0.76	
FINER [17]	122	83.84	0.76	
Gauss [23]	134	105.88	0.76	
GaussianImage [34]	236	5187.82	0.074	
MiraGe [32]	299	358.07	109.82	
GaINeR (our)	792	2.50	51.43	

Table 3. Training time, inference speed, and model size for GaINeR and baseline models. All methods were trained on the DIV2K dataset [2] downscaled $3\times$ with bicubic filtering to satisfy input-size requirements across architectures.

7.7. Ablation study

We conduct an ablation study on the KODAK dataset to evaluate the effect of key design parameters in GaINeR. Specifically, we analyze the impact of the number of Gaussian components (N_G) , neighborhood size (N_{KNN}) , search radius (r), hashgrid resolution (\mathcal{H}_{res}) , and hash map capacity (H_{size}) on reconstruction quality. Quantitative results are summarized in Table 4.

We observe that the quality of the features obtained from the hashgrid \mathcal{H} has the largest impact on our model's performance. Reducing either the hashgrid resolution \mathcal{H}_{res} or the hash map size \mathcal{H}_{size} results in a substantial drop in PSNR. Another important factor is the number of Gaussians N_G : decreasing N_G by a factor of 5 leads to a threefold reduction in PSNR. Other parameters, such as neighborhood size or search radius, have a much smaller effect on reconstruction quality.

Parameter values				KODAK		
N_G	N_{KNN}	r	\mathcal{H}_{res}	\mathcal{H}_{size}	PSNR	MS-SSIM
250k	16	0.1	8192	21	64.08	0.9999
100k	16	0.1	8192	21	25.02	0.9442
500k	8	0.1	8192	21	77.52	0.9999
500k	4	0.1	8192	21	60.06	0.9999
500k	16	0.1	4096	21	63.47	0.9999
500k	16	0.1	1024	21	41.12	0.9962
500k	16	0.05	8192	21	76.83	0.9999
500k	16	0.2	8192	21	75.94	0.9999
500k	16	0.1	8192	19	62.02	0.9999
500k	16	0.1	8192	17	55.97	0.9999
500k	16	0.1	8192	21	77.09	0.9999

Table 4. Ablation study on the KODAK dataset. We evaluate the influence of the number of Gaussian components (N_G) , number of nearest neighbors (N_{KNN}) , search radius (r), hashgrid resolution (\mathcal{H}_{res}) , and hash map size (\mathcal{H}_{size}) on reconstruction quality. PSNR and MS-SSIM are reported for each configuration. We marked with red changed parameter.

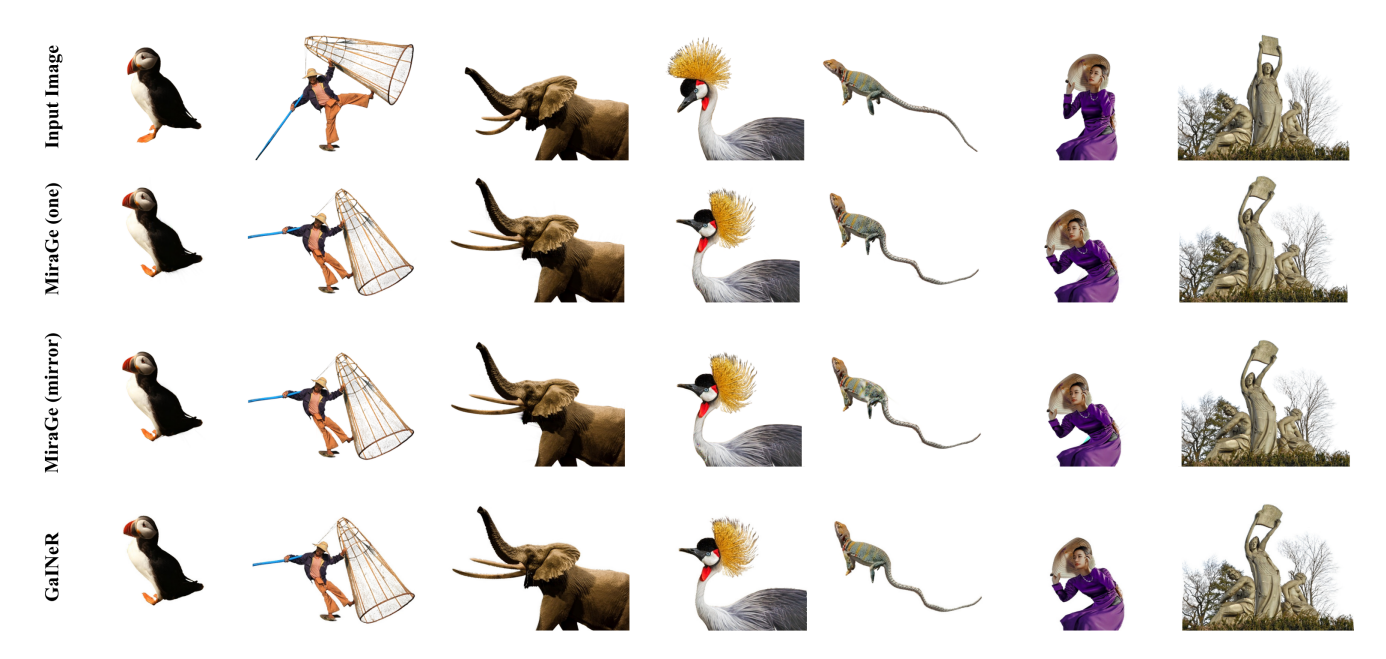


Figure 15. Extended qualitative assessment of MiraGe [32] and GaINeR under manually introduced geometric transformations. Both models handle the fisherman, puffin, and statue scenes equally well. In contrast, MiraGe shows artifacts in several cases: around the woman's abdomen, near the elephant's neck when using the mirror camera, and along the body of the lizard and the neck of the gray crowned crane under the same camera setting.



Figure 16. Visualizations of physics-based simulations. **Top:** An elastic apple deforming under constant gravity upon impact. **Middle:** A bouquet subjected to oscillating lateral forces, demonstrating structural flexibility. **Bottom:** A multi-material simulation showcasing the interaction between a granular object and a fluid volume, demonstrating complex mixing and flow dynamics.